Progress In Electromagnetics Research B, Vol. 53, 1–24, 2013

EFFECTS OF LOCAL PHASE ERRORS IN MULTI-LOOK SAR IMAGES

Oleksandr O. Bezvesilniy, Ievgen M. Gorovyi*, and Dmytro M. Vavriv

Department of Microwave Electronics, Institute of Radio Astronomy of the National Academy of Sciences of Ukraine, 4 Chervonopraporna Str., Kharkov 61002, Ukraine

Abstract—The synthetic aperture radar (SAR) is a widely used instrument for high-resolution imaging from aircraft or satellite platforms. In the paper, the problem of the defocusing of multi-look SAR images by uncompensated phase errors presented in the received data is analyzed. It is shown that the phase errors on a multi-look processing interval can be effectively described in terms of local quadratic and local linear phase errors. Approximate analytical expressions are derived to describe the azimuth resolution degradation. Criteria for acceptable phase errors are given. The obtained results are verified by numerical simulations. The approach is illustrated by two typical motion errors: slow deflections of a SAR platform trajectory from a reference flight line and periodic trajectory deviations.

1. INTRODUCTION

Synthetic aperture radars (SARs) are used in many applications due to their ability to perform high-resolution imaging of Earth's surface [1–4]. The multi-look processing technique is widely used in such systems to suppress the speckle noise and reveal fine details in SAR images [1–3, 5–8], as well as for other applications [9, 10]. The principle of such processing is based on non-coherent averaging of several SAR images of the same scene built from the data collected on different segments of the flight trajectory. Here, as in single-look SARs, the high range resolution is commonly achieved by using a linear frequency modulation (LFM) of the transmitted radar pulses, whereas the high azimuth resolution is obtained by a coherent processing of

Received 30 April 2013, Accepted 6 July 2013, Scheduled 8 July 2013

* Corresponding author: Ievgen M. Gorovyi (gorovoy@rian.kharkov.ua).

the consequent backscattered radar pulses. The knowledge of the actual aircraft trajectory is required to realize such processing. The requirements to the precision of the trajectory measurements are very high. Usually, various autofocus techniques are used to estimate the uncompensated errors in the SAR data [1, 2, 11, 12]. However, despite of all efforts, some uncompensated phase errors are inevitably presented in SAR data leading to a degradation of the SAR image quality [13–20].

The extent of the image quality degradation depends on many factors such as the radar hardware parameters (particularly, the radar wavelength), the reference flight parameters (the flight velocity, the altitude, and the antenna beam orientation), the required azimuth resolution, as well as peculiarities of the phase errors that are typical for the SAR platform and the radar installation, and so on.

The degradation of the SAR image quality can be considered as distortions of the synthetic aperture pattern (SAP), in particular, the broadening of the main lobe and the raising of the side lobes. In this paper, the azimuth resolution degradation (defocusing) is analyzed since this effect is more important than the problem of the side lobes for the multi-look processing, especially for airborne SAR systems [5, 6, 21]. Thus, the influence of the phase errors on the azimuth resolution of multi-look SAR images is analyzed.

A new approach to the representation of an arbitrary phase error function by local linear phase errors (LLPE) and local quadratic phase errors (LQPE) is introduced. These local errors are related to the coefficients of the Taylor series expansions of the error function on the time intervals comparable to the time of the single-look synthesis. Such local consideration is shown to be useful for the analysis of the distortions of the multi-look SAP. The comprehensive analysis of the resolution degradation of the multi-look SAP is provided.

The known approaches to the low-frequency phase error analysis [1, 2, 14] typically use various models (quadratic, cubic, polynomial, harmonic errors, etc.) to describe such errors. We shall show that it is sufficient to introduce only local linear and local quadratic phase errors in order to describe qualitatively and quantitatively the effect of all types of low-frequency errors on multi-look SAR images. The proposed approach allows to reveal the nature of phase errors in particular SAR images and to develop approaches to their compensation.

The paper is organized as follows. In Section 2, the idea of the phase error local approximations is described. The defocusing of the single-look SAP by the LLPE and LQPE is examined in Section 3. The influence of the LLPE and LQPE on the multi-look SAP is analyzed

in Section 4. Approximate analytical expressions for the degradation of the azimuth resolution are derived and criteria for the acceptable phase errors are given both for the LQPE and LLPE. The obtained relations are supported by numerical simulations. The application of the proposed approach is illustrated on two typical cases of the phase errors:

1) The quadratic phase error on a multi-look processing interval (Section 5) that represents slow deflections of the SAR platform trajectory from the reference flight line.
2) The harmonic phase error (Section 6) that describes periodic trajectory deviations induced, for example, by an autopilot operation or by a cross-track antenna motion due to the aircraft roll motion.

Section 7 illustrates the described effects of the phase errors on multi-look SAR images in the case of real SAR data processing.

2. MULTI-LOOK SAR PROCESSING AND LOCAL APPROXIMATION OF PHASE ERRORS

The formation of the synthetic aperture is a kind of matched filtering [1, 3]. It can be represented as the convolution of the received radar signal $s(t)$ with the reference function $h(t)$ in the time domain. For the multi-look processing, several SAR images (called SAR looks) are formed by dividing the reference function on segments of the duration T_S (the single-look interval of synthesis) centered at the moments of time t_L:

$$I_{SL}(t, t_L) = \left| \frac{1}{T_S} \int\limits_{-T_S/2}^{T_S/2} s(t+\tau+t_L) w(\tau/T_S) h(\tau+t_L) d\tau \right|^2 . \quad (1)$$

Here $I_{SL}(t, t_L)$ is the azimuth line of the SAR look with the index L, $L = 0, \pm 1, \pm 2, \ldots, \pm N_L/2$, where N_L is the number of looks (an odd number). The azimuth time t is related to the azimuth position of an aircraft $X = Vt$ on the reference flight line. V is the aircraft flight velocity. In signal processing schemes with non-overlapping intervals. The central moments are determined as $t_L = LT_S$. The time of synthesis T_S determines the azimuth resolution. The maximum number of the looks is limited by the maximum observation time of a ground target. The weighting window $w(\tau/T_S)$ is applied to control the level of the side lobes of the synthetic aperture pattern (SAP). A

multi-look SAR image is built by averaging all SAR looks to suppress the speckle noise:

$$I_{ML}(t) = \frac{1}{N_L} \sum_{L=-N_L/2}^{N_L/2} I_{SL}(t, t_L). \tag{2}$$

Actually, the SAR processing is a two-dimensional procedure, and the convolution (1) should be calculated for the signal taken along the range migration curves [1, 3]. However, in this paper we shall assume that uncompensated trajectory deviations responsible for the phase errors in the received data are so small that the range cell migration correction (RCMC) is performed accurately. In this case, the problem of the azimuth resolution degradation can be considered in the azimuth direction only.

In order to derive an expression describing the synthetic aperture pattern (SAP), one should substitute a point target signal into the convolution (1). The received signal and the reference function are usually considered as signals with the linear frequency modulation (LFM) on the Doppler frequency [1, 3]:

$$s(t) = \exp\left[2\pi i \left(F_{DC}t + F_{DR}t^2/2\right) + i\varphi_E(t)\right], \tag{3}$$

$$h(\tau) = \exp\left[-2\pi i \left(F_{DC}\tau + F_{DR}\tau^2/2\right)\right]. \tag{4}$$

Here F_{DC} is the Doppler centroid, and F_{DR} is the Doppler rate. The term with $\varphi_E(t)$ represents the phase error in the received signal.

We shall assume that the phase error is a low-frequency error with respect to the synthesis time T_S so that its highest frequency $f_E^{\max}$ is limited by

$$f_E^{\max} T_S < 1. \tag{5}$$

However, for the whole multi-look time processing interval

$$-T_{ML}/2 \le t \le T_{ML}/2, \quad T_{ML} = T_S N_L, \tag{6}$$

the phase error function $\varphi_E(t)$ can be considered as an arbitrary function. Such behavior of the phase error is typical for many practical airborne SAR systems. Under the assumption (5), the phase error can be approximated as

$$\varphi_E(t + \tau + t_L) \approx \varphi_E(t_L) + \varphi'_E(t_L)(t + \tau) + \varphi''_E(t_L)(t + \tau)^2/2. \tag{7}$$

This approximation is valid on short time intervals of the order of T_S centered at the moments of time $t + t_L$, and in this sense it is a local approximation of the phase error. The constant phase term $\varphi_E(t_L)$ does not affect the SAP. The linear phase error term $\varphi'_E(t_L)(t + \tau)$ shifts the synthetic pattern (or, in other words, declines the synthetic

beam) of this look. The quadratic phase error term $\varphi''_E(t_L)(t+\tau)^2/2$ leads to broadening (defocusing) of the main lobe of the SAP.

Thus, we introduce two types of the local phase errors in our consideration:

1) The local linear phase error (LLPE)

$$\alpha_{EL} = \alpha_E(t_L) = \frac{1}{2\pi}\varphi'_E(t_L)T_S, \tag{8}$$

2) The local quadratic phase error (LQPE)

$$\beta_{EL} = \beta_E(t_L) = \frac{1}{2\pi}\varphi''_E(t_L)T_S^2. \tag{9}$$

The LLPE and LQPE affect the SAP in different ways, and their accounting is principally important for the multi-look processing.

The time of the single-look synthesis T_S, which is the characteristic time of the local approximation (7), is used to introduce dimensionless LLPE (8) and LQPE (9). For the convenience sake, we also introduce the following dimensionless parameters:

$$\xi = \tau/T_S, \quad \eta = F_{DR}T_S t, \quad \alpha_{DC} = F_{DC}T_S, \quad \beta_{DR} = F_{DR}T_S^2. \tag{10}$$

Note that the dimensionless azimuth coordinate η is related to the azimuth coordinate X as

$$\eta = F_{DR}T_S X/V. \tag{11}$$

By substituting the signal (3) and the reference function (4) into the convolution integral (1), accounting the phase error approximation (7) and introducing the dimensionless notations (8)–(10), the following convenient expression for the SAP is derived:

$$I_{SL}(\eta, \alpha_{EL}, \beta_{EL}) = \left| \int_{-1/2}^{1/2} w(\xi) \exp\left[2\pi i \left\{\alpha_{EL} + \left(1 + \frac{\beta_{EL}}{\beta_{DR}}\right)\eta\right\}\xi\right] \exp[\pi i \beta_{EL}\xi^2] d\xi \right|^2. \tag{12}$$

The influence of the local phase errors is illustrated in Fig. 1. The dash curves depict synthetic beams in the error-free case. The solid curves in the figure show the beam distortions for three cases: the declination of a beam caused by the LLPE (Fig. 1(a)), the defocusing (the broadening) of a beam due to the LQPE (Fig. 1(b)), and both the declination and the defocusing of a beam in the presence of the both types of the local phase errors (Fig. 1(c)). Thus, each of SAR looks is distorted by its own LLPE α_{EL} and LQPE β_{EL} before being summed up into a multi-look SAP. The dominating impact of the LLPE or

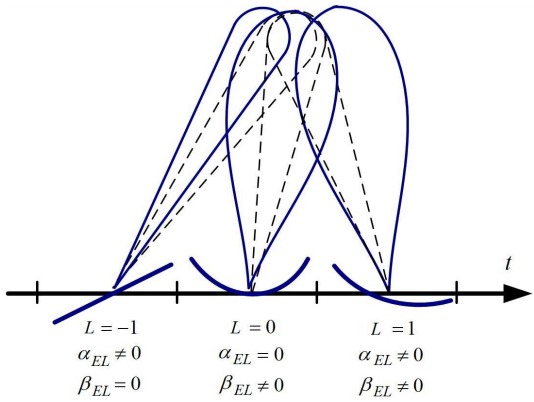

Figure 1. The influence of the local phase errors on SAR look beams.

LQPE depends on the behavior of the phase error on the multi-look processing interval.

As far as the phase error is assumed to be a low-frequency error as compared to the synthesis time (5), the effect of the side lobes is insignificant for the overall SAR image quality, and, therefore, it will not be considered in this paper.

The azimuth resolution is typically defined as the 3-dB-level width of the main lobe of the SAP. However, in the case of strong phase errors, the main lobe can be significantly distorted, and the 3-dB-level definition cannot be applied effectively. Instead, the main lobe width can be adequately characterized by the integral resolution defined as

$$\rho = \frac{1}{I_{SL/ML}^{\max}} \int_{-\infty}^{\infty} I_{SL/ML}(\eta) d\eta, \tag{13}$$

where $I_{SL/ML}^{\max}$ is the maximum value of the SAP.

In the error-free case, $\alpha_{EL} = 0$ and $\beta_{EL} = 0$, the synthetic aperture pattern (12) does not depend on the look index L and takes the following simple form:

$$I(\eta) = \left| \int_{-1/2}^{1/2} w(\xi) \exp\left[2\pi i \eta \xi\right] d\xi \right|^2 . \tag{14}$$

For the rectangular window $w_R(\xi)$

$$w_R(\xi) = \begin{cases} 1, & |\xi| \le 1/2, \\ 0, & |\xi| > 1/2, \end{cases} \tag{15a}$$

and for the Hamming window $w_H(\xi)$,

$$w_H(\xi) = \begin{cases} 1 + (23/27)\cos(2\pi\xi), & |\xi| \le 1/2 \\ 0, & |\xi| > 1/2. \end{cases} \tag{15b}$$

normalized so that

$$\left| \int_{-1/2}^{1/2} w_{R,H}(\xi) d\xi \right|^2 = 1, \tag{16}$$

one can derive the following explicit expressions for the SAPs:

$$I_R(\eta) = \left| \frac{\sin(\pi\eta)}{\pi\eta} \right|^2, \tag{17a}$$

$$I_H(\eta) = \left| \frac{\sin(\pi\eta)}{\pi\eta} \right|^2 \left[\frac{1 - \eta^2(4/27)}{1 - \eta^2} \right]^2. \tag{17b}$$

The integral resolution (13) for the SAPs (17) is, respectively,

$$\rho_R = 1.0, \tag{18a}$$

for the rectangular window, and

$$\rho_H \approx 1.363, \tag{18b}$$

for the Hamming window. The corresponding 3-dB resolutions are $\rho_R^{3\,\mathrm{dB}} \approx 0.886$ and $\rho_H^{3\,\mathrm{dB}} \approx 1.30$. The azimuth resolution in meters can be easily found from (11) via the following relation

$$\rho_{XR/H} = \rho_{R/H} \frac{V}{|F_{DR}| T_S}. \tag{19}$$

The application of the weighting window reduces the side-lobes level and broadens the main lobe of the synthetic aperture pattern. The dimensionless integral resolution $\rho_{R/H}$ is, actually, the broadening factor of the main lobe.

3. INFLUENCE OF LLPE AND LQPE ON THE SINGLE-LOOK SAP

In this section, the influence of the LLPE and LQPE on the single-look SAP is analyzed, and criteria for acceptable phase errors are given. The consideration is based on the expression (12).

The LLPE α_{EL} appears in (12) in the linear phase term with respect to ξ. The presence of the LLPE does not deteriorate the

resolution of the single-look SAP but only shifts it so that the maximum of the SAP is located at

$$\eta_L(\alpha_{EL}, \beta_{EL}) = -\frac{\alpha_{EL}}{1 + \beta_{EL}/\beta_{DR}}. \tag{20}$$

The position of the maximum depends not only on the LLPE α_{EL} itself but also on the ratio of the LQPE β_{EL} to the dimensionless Doppler rate β_{DR}. It is assumed that that the LQPE β_{EL} is relatively small, so that $|\beta_{EL}/\beta_{DR}| < 1$. The value of β_{DR} is always negative and its absolute value is the time-bandwidth product (TBP) of the processed signal. Depending on the sign of the LQPE β_{EL} the shift caused by the LLPE α_{EL} can be intensified (if $\beta_{EL} > 0$) or weakened (if $\beta_{EL} < 0$).

If the shift of the SAP maximum (20) on the half of the resolution cell is assumed to be an acceptable error then the simple criterion for the acceptable LLPE can be written

$$|\eta_L(\alpha_{EL}, \beta_{EL})| < \rho_{R/H}/2. \tag{21}$$

The defocusing effect of the LQPE on the single-look SAP does not depend on the LLPE. Therefore, while considering the LQPE we can assume that the LLPE is zero, $\alpha_{EL} = 0$. Under this assumption the expression (12) can be written as

$$I_{SL}(\eta,\beta_{EL}) = \left| \int_{-1/2}^{1/2} w(\xi) \exp\left[2\pi i \left(1 + \frac{\beta_{EL}}{\beta_{DR}}\right)\eta\xi\right] \exp\left[\pi i \beta_{EL} \xi^2\right] d\xi \right|^2 . \tag{22}$$

The LQPE affects the SAP in two ways. First, the LQPE appears in the coefficient $(1 + \beta_{EL}/\beta_{DR})$ in the linear phase term with respect to ξ in (22). This coefficient is a scaling factor: it stretches or contracts the SAP in the azimuth coordinate η. This linear scaling effect essentially depends on the TBP value β_{DR}. Second, the LQPE appears in the quadratic phase term with respect to ξ in (22). This term describes the quadratic defocusing effect. Both terms contribute to a degradation of the SAP.

A more in-depth analytical investigation of the SAP degradation based on (22) is complicated; and further analysis was performed numerically. The results on the degradation of the SAP caused by the LQPE are presented in Fig. 2 for high and low values of β_{DR}. The rectangular and Hamming weighting windows are considered.

For high values of the TBP, for example for $\beta_{DR} = -200$ (Figs. 2(a) and 2(b)), the broadening of the SAP is mainly determined by the quadratic defocusing effect (the quadratic phase term in (22)). In this case, the SAP degradation is symmetrical with respect to the sign of the LQPE β_{EL}. For low values of the TBP, for example for

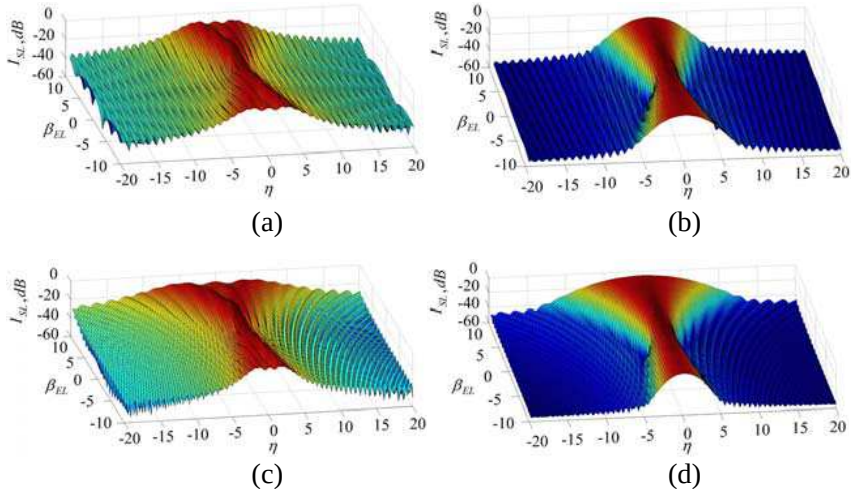

Figure 2. The degradation of the SAP caused by the LQPE in the cases of (a), (b) the high TBP value ($\beta_{DR} = -200$) and (c), (d) the low TBP value ($\beta_{DR} = -20$) for (a), (c) the rectangular window and (b), (d) the Hamming window.

$\beta_{DR} = -20$ (Figs. 2(c) and 2(d)), the degradation of the SAP depends also on the linear scaling effect (the linear phase term in (22)), and the SAP behavior depends on the sign of the LQPE β_{EL} (stretching or contracting in the azimuth direction).

One can note oscillations on the highly defocused main lobe of the SAP when the rectangular window is used (Figs. 2(a) and 2(c)). The application of the Hamming window results in smoothing of these ripples (Figs. 2(b) and 2(d)).

Disregarding the oscillations that appear in the case of the rectangular window, the maximum value of the SAP is achieved at $\eta = 0$. This maximum value is determined by the following expression:

$$I_{SL}^{\max}(\beta_{EL}) = I_{SL}(0, \beta_{EL}) = \left| \int_{-1/2}^{1/2} w(\xi) \exp[\pi i \beta_{EL} \xi^2] d\xi \right|^2 . \quad (23)$$

It should be noted that the degradation of the maximum value is completely determined by the quadratic defocusing effect (the quadratic phase term in (22)). The degradation can be analyzed both numerically and analytically. Assuming that the LQPE is small and expanding the quadratic-phase exponent in a series up to the second-order terms as

$$\exp\left[\pi i \beta_{EL} \xi^2\right] \approx 1 + i\pi\beta_{EL}\xi^2 - \left(\pi\beta_{EL}\xi^2\right)^2 / 2 \quad (24)$$

one can find from (23) the following approximations for the SAP maximum for the rectangular window and for the Hamming window, respectively:

$$I^{\max}_{SLR/H}(\beta_{EL}) \approx \frac{1}{1+k_{R/H}\beta^2_{EL}}, \quad k_R = 0.055, \quad k_H = 0.024. \tag{25}$$

These analytical approximations are compared with numerical computations in Fig. 3, and a rather good correspondence of these results should be noted.

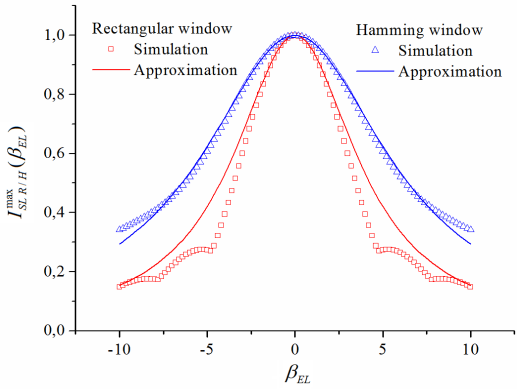

Figure 3. The degradation of the SAP maximum value caused by the LQPE.

Substituting (22) into the definition of the azimuth resolution (13), after some transformations we find

$$\rho(\beta_{EL}) = \frac{1}{\left(1+\frac{\beta_{EL}}{\beta_{DR}}\right)} \frac{\int\limits_{-1/2}^{1/2} [w(\xi)]^2 d\xi}{\left| \int\limits_{-1/2}^{1/2} w(\xi) \exp\left[\pi i \beta_{EL} \xi^2\right] d\xi \right|^2}. \tag{26}$$

The numerator represents just the error-free integral resolution values (18):

$$\rho_{R/H} = \int\limits_{-1/2}^{1/2} [w_{R/H}(\xi)]^2 d\xi. \tag{27}$$

The two factors in the denominator in (26) represent exactly the linear scaling effect and the quadratic defocusing effect. Substituting (25)

into (26) we obtain analytical expressions for the resolution

$$\rho_{R/H}(\beta_{EL}) = \rho_{R/H}\frac{1 + k_{R/H}\beta_{EL}^2}{1 + \beta_{EL}/\beta_{DR}} \tag{28}$$

for the rectangular and the Hamming windows, respectively. These approximate analytical dependences are shown in Fig. 4 along with results of numerical calculations. From this figure one can see that the expressions (28) can be used at least for $|\beta_{EL}| \leq 10$.

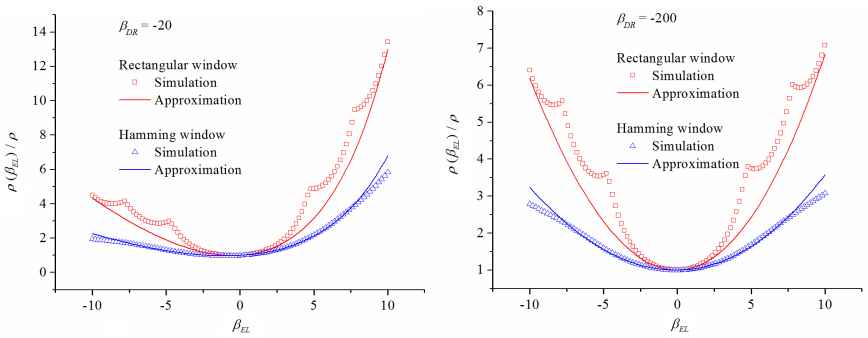

Figure 4. The degradation of the azimuth resolution caused by the LQPE for (a) the low TBP and (b) the high TBP values.

If the linear scaling effect can be neglected (when $|\beta_{EL}/\beta_{DR}| \ll 1$) then the quadratic defocusing effect dominates and the following simple numerical criteria for the acceptable LQPE can be found. For example, a 25% resolution degradation corresponds to

$$I_{SLR/H}^{\max}\left(\beta_{ELR/H}^{25\%}\right) = 0.8, \quad \beta_{ELR}^{25\%} \approx 2.0, \quad \beta_{ELH}^{25\%} \approx 3.2, \tag{29a}$$

and a 2-times resolution degradation corresponds to

$$I_{SLR/H}^{\max}\left(\beta_{ELR/H}^{\times 2}\right) = 0.5, \quad \beta_{ELR}^{\times 2} \approx 3.5, \quad \beta_{ELH}^{\times 2} \approx 6.3. \tag{29b}$$

A more general criterion for the acceptable LQPE can be found analytically from (28). For example, for the Hamming window, it yields

$$\beta_{ELR/H}^{TH}(\Delta\rho, \beta_{DR}) = \frac{\frac{1+\Delta\rho}{\beta_{DR}} \pm \sqrt{\left(\frac{1+\Delta\rho}{\beta_{DR}}\right)^2 + 4k_{R/H}\Delta\rho}}{2k_{R/H}}, \tag{30}$$

where $\Delta\rho = 1 - \rho(\beta_{EL}^{TH})/\rho$ is the relative resolution degradation.

The resolution degradation has also been investigated numerically and the results are given in Fig. 5. One can observe that for low values

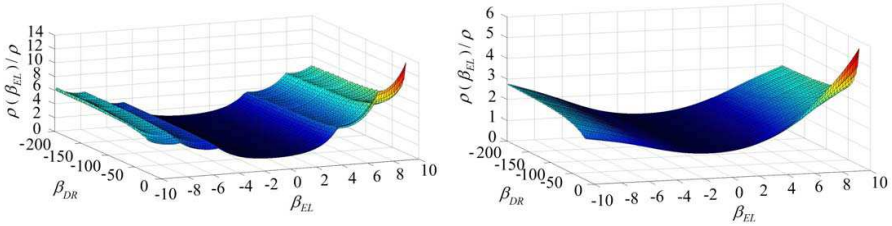

Figure 5. Degradation of the azimuth resolution versus the β_{EL} and β_{DR}, (a) for the rectangular window, and (b) for the Hamming window.

of β_{DR} the resolution degrades faster for positive values of the LQPE β_{EL} due to the scaling effect. For high values of β_{DR}, the resolution degradation becomes insensitive to the sign of the LQPE, and it is determined mainly by the quadratic defocusing effect.

4. INFLUENCE OF LLPE AND LQPE ON MULTI-LOOK SAP

The multi-look SAP is built by averaging the single-look SAPs of all SAR looks. Each of the single-look SAPs is shifted by its LLPE according to (20) and defocused by its LQPE according to (28). The presence of different LLPEs on the multi-look processing interval leads to an additional degradation of the resolution of the multi-look SAP, and this effect can even dominate over the LQPE defocusing effect.

In order to analyze the defocusing effect of the LLPEs, we shall assume that all single-look SAPs are defocused by the same LQPE β_E which corresponds to the worst LQPE defocusing effect among all SAR looks. We shall also assume that many looks are summed up and their LLPEs and the shifts (20) are randomly and uniformly distributed within the given intervals:

$$|\alpha_{EL}| \le \alpha_{E\max}, \quad |\eta_L(\alpha_{EL}, \beta_E)| \le \eta_{E\max}. \tag{31}$$

Such a mathematical model allows us to find an approximate analytical solution that describes the influence of the LLPEs on the resolution of the multi-look SAP.

Following the definitions of the multi-look SAP (2) and the integral resolution (13), the multi-look resolution can be determined as

$$\rho_{ML}(\alpha_{E\max}, \beta_E) = \frac{\int\limits_{-\infty}^{\infty} I_{ML}(\eta, \alpha_{E\max}, \beta_E) d\eta}{I_{ML}^{\max}(\alpha_{E\max}, \beta_E)}, \tag{32}$$

$$I_{ML}(\eta, \alpha_{E\max}, \beta_E) = \frac{1}{N_L} \sum_{L=-N_L/2}^{N_L/2} I(\eta, \alpha_{EL}, \beta_E). \tag{33}$$

Changing the order of the integration and summation in the numerator of (32) and taking into account that for each single-look SAP (see (26)–(27))

$$\int_{-\infty}^{\infty} I(\eta, \alpha_{EL}, \beta_E) d\eta = \rho(\beta_E) I_{SL}^{\max}(\beta_E) = \frac{\rho}{1 + \beta_E/\beta_{DR}}, \tag{34}$$

one can easily find the numerator of (32):

$$\begin{aligned} \int_{-\infty}^{\infty} I_{ML}(\eta, \alpha_{E\max}, \beta_E) d\eta &= \frac{1}{N_L} \sum_{L=-N_L/2}^{N_L/2} \int_{-\infty}^{\infty} I(\eta, \alpha_{EL}, \beta_E) d\eta \\ &= \frac{\rho}{1 + \beta_E/\beta_{DR}}. \end{aligned} \tag{35}$$

By using the above introduced mathematical model of the uniformly distributed shifts, the maximum of the multi-look SAP (the denominator of (32)) can be estimated as the averaged value of the maximum of the single-look SAP on the interval (31) as

$$\begin{aligned} I_{ML}^{\max}(\alpha_{E\max}, \beta_E) &= \max \left[\frac{1}{N_L} \sum_{n_L=-N_L/2}^{N_L/2} I(\eta, \alpha_{EL}, \beta_E) \right] \\ &\approx \frac{1}{2\eta_{E\max}} \int_{-\eta_{E\max}}^{\eta_{E\max}} I(\eta, \beta_E) d\eta. \end{aligned} \tag{36}$$

In order to perform the integration in (36) analytically, we introduce the following approximation for the single-look defocused SAP:

$$I_{SL}^{Approx}(\eta, \beta_E) \approx \begin{cases} I_{SL}^{\max}(\beta_E) \left[1 - \left(\frac{\eta}{(3/4)\rho(\beta_E)} \right)^2 \right] & \text{if } |\eta| < (3/4)\rho(\beta_E), \\ 0 & \text{otherwise.} \end{cases} \tag{37}$$

The maximum values of this approximate SAP (at $\eta = 0$) is equal exactly to the true maximum $I_{SL}^{\max}(\beta_E)$ of the single-look SAP (25). The coefficient 3/4 is introduced in (37) so that the integral resolution of the approximate SAP is equal to the corresponding actual resolution $\rho(\beta_E)$ of the single-look SAP (28). By using such simple and convenient approximation the integration in (36) can be

easily performed analytically. Finally, we obtain the following explicit expression for the degradation of the maximum of the multi-look SAP:

$$I_{ML}^{\max}(\eta_{E\max},\beta_E) \approx \begin{cases} I_{SL}^{\max}(\beta_E)\left[1-\frac{1}{3}\left(\frac{\eta_{E\max}}{(3/4)\rho(\beta_E)}\right)^2\right] & \text{if } |\eta_{E\max}|<(3/4)\rho(\beta_E), \\ I_{SL}^{\max}(\beta_E)\frac{\rho(\beta_E)}{2\eta_{E\max}} & \text{otherwise.} \end{cases} \quad (38)$$

Combining (34), (35) and (38), the multi-look SAP resolution can be written as

$$\rho_{ML}(\eta_{E\max},\beta_E)\approx\begin{cases}\frac{\rho(\beta_E)}{1-\frac{1}{3}\left(\frac{\eta_{E\max}}{(3/4)\rho(\beta_E)}\right)^2} & \text{if } |\eta_{E\max}|<(3/4)\rho(\beta_E), \\ 2\eta_{E\max} & \text{otherwise.}\end{cases} \quad (39)$$

For small values of the LLPE, the multi-look resolution is equal to the resolution of the single-look SAP. With the growth of the LLPE up to the approximate threshold of $|\eta_{E\max}| < (3/4)\rho(\beta_E)$, the LLPE and LQPE both make comparable contributions into the defocusing effect. Above this threshold, the LLPE degradation starts to dominate over the pure LQPE defocusing.

The behavior of the multi-look resolution is illustrated in Fig. 6. The solid curves represent the approximate analytical solution (39). Fig. 6(a) shows the resolution versus $\alpha_{E\max}$ for the fixed $\beta_E = 2$. Fig. 6(b) shows resolution versus β_E for the given $\alpha_{E\max} = 0.5$. The boxes in these figures show the resolution values obtained numerically using the above-introduced statistical model of the uniformly distributed SAP shifts. The figures are built for the Hamming window. These images prove the validity of the approximations.

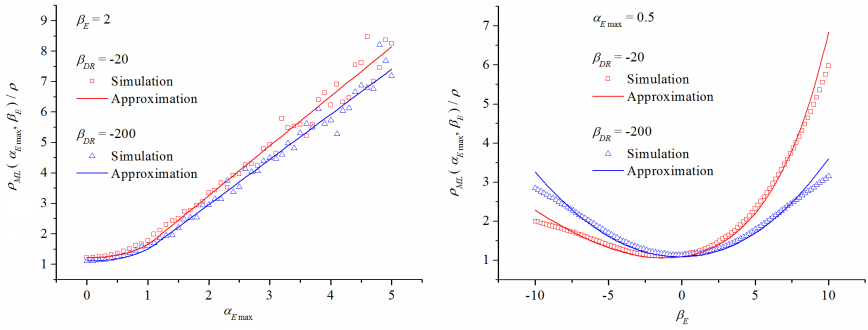

(a) (b)

Figure 6. The degradation of the resolution of the multi-look SAP (a) versus $\alpha_{E\max}$ and (b) versus β_E.

5. QUADRATIC PHASE ERROR ON MULTI-LOOK INTERVAL

The slow deflection of the SAR platform trajectory from the reference flight line is a typical case of the uncompensated motion error. The corresponding phase error can be approximated as a quadratic phase error defined on the multi-look processing interval:

$$\varphi_E(t) \approx \pi\beta_p(t/T_S)^2. \tag{40}$$

The LLPE and LQPE for the centers of the looks $t_L = LT_S$ are given by

$$\alpha_{EL} = \beta_p L, \quad \beta_{EL} = \beta_p\,. \tag{41}$$

The LLPE grows while going from the center of the multi-look processing interval, and the LQPE is constant. The local approximation is explained in Fig. 7.

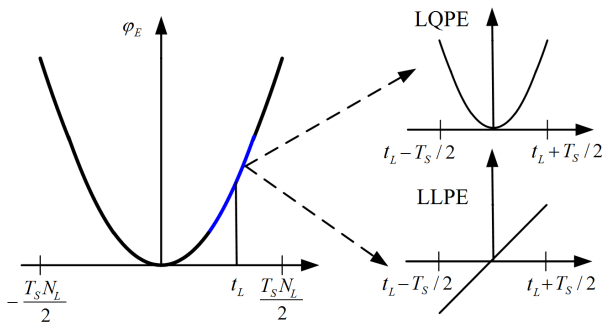

Figure 7. The quadratic phase error on the multi-look processing interval.

The resolution of the multi-look SAP is described by the solution (39) if the shift between consequent looks t_L and t_{L+1} does not exceed the resolution cell. It means that

$$|\beta_p| < 1. \tag{42}$$

This requirement guarantees that there are no oscillations on the main lobe of the multi-look SAP, and the model with the uniformly distributed shifts of the single-look SAPs is valid. The parameters in (39) are as follows:

$$\alpha_{E\max} = |\beta_p|\, N_L/2, \quad \eta_{L\max} = \frac{\alpha_{E\max}}{1+\beta_p/\beta_{DR}}, \quad \beta_E = \beta_p. \tag{43}$$

From (42) and from the LQPE acceptable error criteria (29) we find that for a large number of looks the LLPE dominates over the

LQPE. Moreover, the resolution becomes simply proportional to the number of looks:

$$\rho_{ML}(N_L, \beta_p) \approx 2\eta_{E\max} = \frac{|\beta_p|\, N_L}{1 + \beta_p/\beta_{DR}}. \tag{44}$$

This property can be used to detect the quadratic phase error in the received SAR data. If we increase the number of looks and obtain the proportional degradation of the azimuth resolution in the multi-look SAR image, it means that the quadratic phase error (40) is presented on the multi-look processing interval.

The multi-look SAPs built of 3 looks and 9 looks versus the quadratic phase error β_p are shown in Fig. 8. One can observe that for the low TBP case (Figs. 8(c), 8(d)) the defocusing depends on the sign of β_p. Such behavior is caused by the stretching effect that was examined above. Also, one can see that for the large error values (approximately for $|\beta_p| > 2$) the main lobe of the multi-look SAP falls apart onto several maxima that correspond to the shifted single-look SAPs.

The degradation of the resolution of the multi-look SAP caused by the quadratic phase error versus the number of looks is shown in Fig. 9. The linear proportionality of the resolution degradation to the number of looks (44) is clearly seen. Also, the above-mentioned asymmetry of the degradation with respect to the sign of the error β_p is observed in Fig. 9(a).

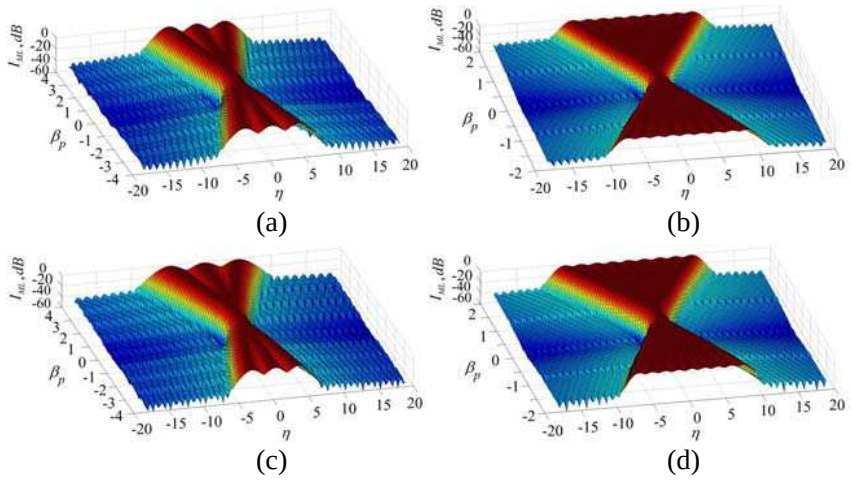

Figure 8. The multi-look SAPs ((a), (c) 3 looks and (b), (d) 9 looks) versus the quadratic phase error presented on the multi-look processing interval for (a), (b) a high TBP and (c), (d) low TBP.

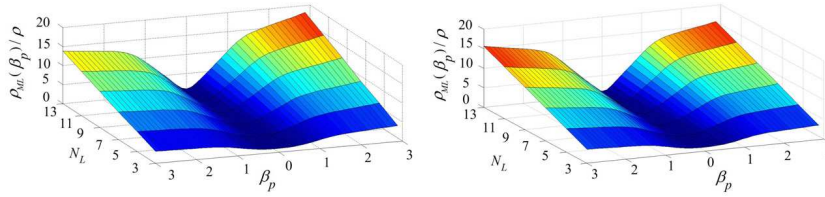

(a) (b)

Figure 9. The degradation of the resolution of the multi-look SAP caused by the quadratic phase error on the multi-look processing interval versus the number of looks for the (a) low TBP and (b) high TBP cases.

6. HARMONIC PHASE ERROR ON MULTI-LOOK PROCESSING INTERVAL

In this section, we consider the defocusing effect of a harmonic phase error determined on the multi-look processing interval. The error is described as

$$\varphi_E(t) = \Phi_p \sin(2\pi F_p t). \tag{45}$$

Here Φ_p is the amplitude and F_p the frequency of the harmonic error. Such phase error describes periodic trajectory deviations induced, for example, by an autopilot operation or by a cross-track antenna motion due to the aircraft roll motion.

The LLPE and LQPE of the harmonic error at the moment of time t_L are given by

$$\alpha_{EL} = \frac{1}{2\pi}\varphi'_E(t_L)T_S = (F_pT_S)\Phi_p \cos(2\pi F_p t_L), \tag{46}$$

$$\beta_{EL} = \frac{1}{2\pi}\varphi''_E(t_L)T_S^2 = -2\pi(F_pT_S)^2\Phi_p \sin(2\pi F_p t_L). \tag{47}$$

The maximum LLPE is reached when the LQPE is zero (the most shifted looks are not defocused), and vice versa, the maximum LQPE is reached when the LLPE is zero (the most defocused looks are not shifted).

It is convenient to introduce the dimensionless frequency as

$$\alpha_p = F_pT_S. \tag{48}$$

The local phase error consideration is valid if the synthesis interval is shorter that the half-period of the harmonic error $T_S < 1/(2F_p)$. Also, the period of the harmonic error should be less than the length of the multi-look processing interval, $1/F_p < T_{ML}$. Thus, the appropriate values of the dimensionless frequency of the harmonic phase error are

$$1/N_L \le \alpha_p \le 1/2. \tag{49}$$

The extreme values of the LLPE and LQPE observed on the multi-look processing interval are $\pm\alpha_{E\max}$ and $\pm\beta_{E\max}$,

$$\alpha_{E\max} = \alpha_p \Phi_p, \tag{50a}$$

$$\beta_{E\max} = 2\pi\alpha_p^2 \Phi_p = 2\pi\alpha_p \alpha_{E\max}. \tag{50b}$$

Since the maximum LLPE and LQPE are determined only by the amplitude and the frequency of the phase error, the defocusing effect of the harmonic phase error does not depend on the number of looks.

The resolution degradation of the multi-look SAP in the case of the harmonic phase error was obtained by numerical simulations, and it is illustrated in Fig. 10. The resolution is the function of two variables: the frequency α_p and the LLPE $\alpha_{E\max}$. From Fig. 10 it is seen that the resolution slightly depends on the frequency α_p of the harmonic error, if the value of $\alpha_{E\max}$ is kept constant, provided the amplitude Φ_p is inversely proportional to the frequency according to (50a). The slight degradation of the resolution with the frequency is caused by the growing $\beta_{E\max}$ (50b).

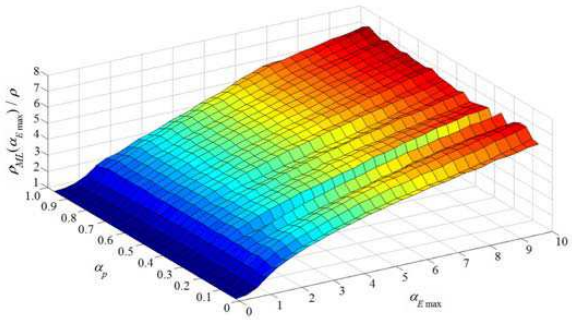

Figure 10. The resolution degradation of the multi-look SAP in the case of the harmonic error (numerical simulations).

The resolution as the function of $\alpha_{E\max}$ for the given frequency $\alpha_p = 0.25$ is shown in Fig. 11 along with the approximation (39) represented by the solid curve.

Strictly speaking, the assumption of the uniform distribution of the LLPE shifts used to derive (39) is not valid for the harmonic error. Actually, the phase $\varphi_L = 2\pi F_p t_L$ in (46)–(47) is uniformly distributed within the interval $[-\pi, \pi]$ but not the LLPEs (46). It means that in order to calculate the maximum of the multi-look SAP, we should average the single-look SAPs shifted by the LLPEs (46) and broadened by the LQPE (47) based on the uniformly distributed phase instead of using the simple averaging (36).

Note that the uniform distribution of the single-look SAP shifts leads to the flat and smooth maximum of the multi-look SAP. Non-uniform distributions lead to peaks on the SAP as those shown in Fig. 12 for the case of the harmonic error. The integral resolution depends on the way how the SAP maximum value is chosen. In the calculations presented in Fig. 11, the mean value between the true maximum $I_{ML}^{\max}$ (in the peaks) and the central value $I_{ML}(0)$ is used as the SAP maximum. Such choice allows us to compensate in some extent the non-uniform distribution and improves the agreement of the simulation and the approximation.

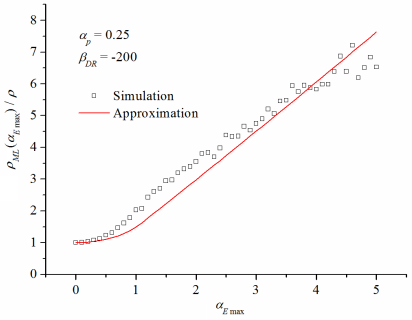

Figure 11. The resolution degradation of the multi-look SAP in the case of the harmonic error as the function of $\alpha_{E\max}$ for $\alpha_p = 0.25$.

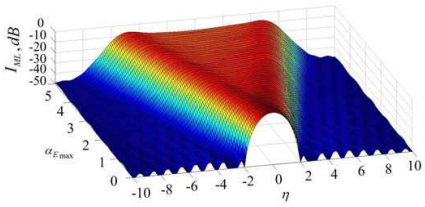

Figure 12. The multi-look SAP degradation in the case of the harmonic error as the function of $\alpha_{E\max}$ for $\alpha_p = 0.25$.

Figure 13. Error-free multi-look SAR image of the scene.

7. THE PHASE ERROR EFFECTS IN SAR IMAGES

In this section, we shall illustrate the described phase error effects by using real SAR data obtained with the X-band airborne SAR system [5, 6].

The SAR image of a test scene is shown in Fig. 13. The image is composed of 31 looks (built from half-overlapped intervals) with a 3-m resolution. Phase errors in the received data were compensated accurately by using the local-quadratic map-drift autofocus (LQMDA) [11, 12]. The scene contains several bright point targets, one of which is indicated by the arrow in the figure. By observing images of such targets it is convenient to illustrate phase errors effects.

In order to demonstrate how the phase errors distort SAR images,

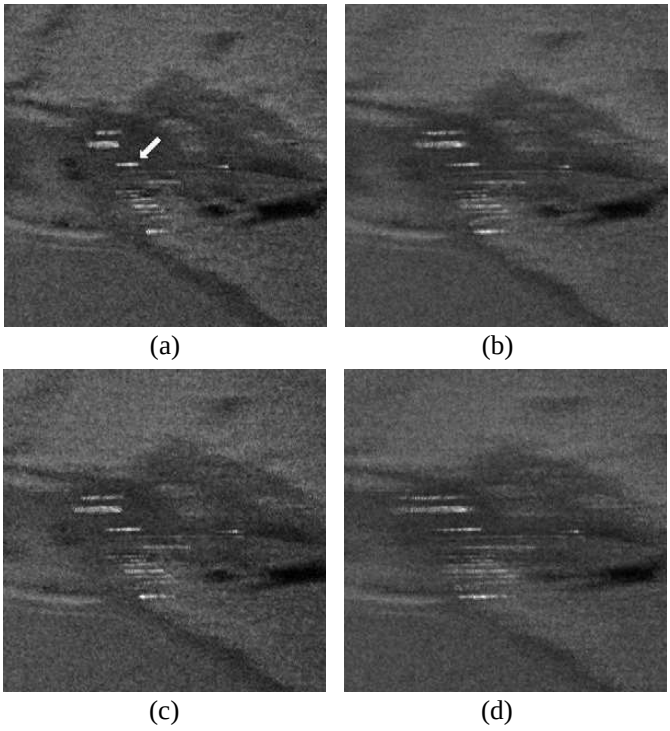

Figure 14. SAR images distorted by the quadratic phase errors introduced on the multi-look processing interval. (a) 15 looks, $2 * pi * \beta_p = 10$. (b) 31 looks, $2 * pi * \beta_p = 10$. (c) 15 looks, $2 * pi * \beta_p = 15$. (d) 31 looks, $2 * pi * \beta_p = 15$.

we intentionally introduce phase errors in the real SAR data for the scene in Fig. 13. Two types of errors are considered: the quadratic phase errors (40) and the harmonic phase error (45) determined on the multi-look processing interval.

Multi-look SAR images built in the presence of the quadratic phase errors are shown in Fig. 14. By comparing the 15-look SAR images in Figs. 14(a) and 14(c) with the 31-look SAR images in Figs. 14(b) and 14(d) one can observe that the resolution degrades proportionally to the number of looks. This effect has been predicted and discussed in Section 5.

Evidently, the larger the error the more significant is the defocusing effect. This can be seen by comparing Figs. 14(a) and 14(b) ($2 * pi * \beta_p = 10$) with Figs. 14(c) and 14(d) ($2 * pi * \beta_p = 15$).

The multi-look SAR images built in the presence of the harmonic

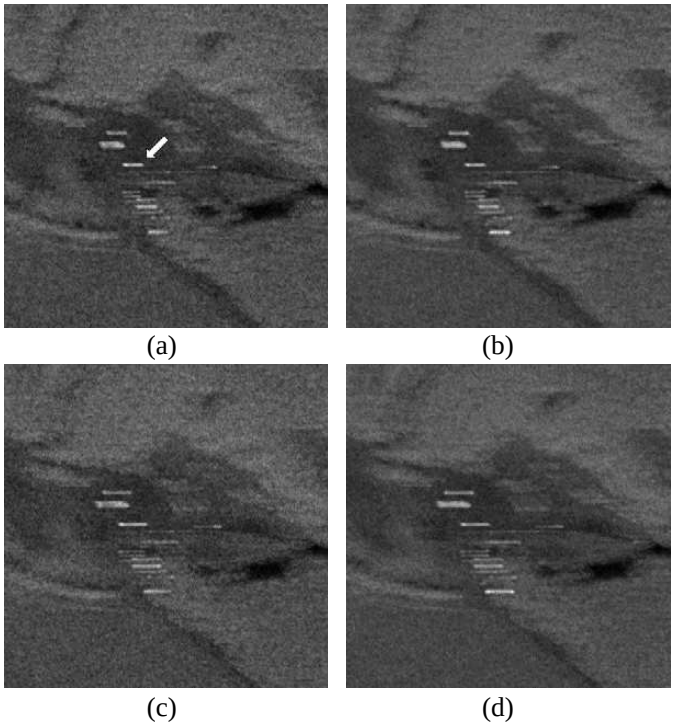

Figure 15. SAR images distorted by the harmonic phase errors with $\alpha_p = 0.3$ introduced on the multi-look processing interval. (a) 15 looks, $\beta_{E\max} = 10$. (b) 31 looks, $\beta_{E\max} = 10$. (c) 15 looks, $\beta_{E\max} = 15$. (d) 31 looks, $\beta_{E\max} = 15$.

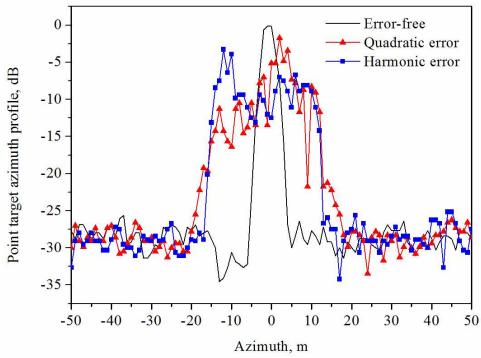

Figure 16. Point target azimuth profiles (taken from Figs. 13, 14(a), and 15(a), for the target indicated by the arrow).

phase errors are shown in Fig. 15. The dimensionless error frequency (48) is $\alpha_p = 0.3$. It means that there are about 3 non-overlapped single-look synthetic aperture intervals within the period of the harmonic phase error. The amplitudes of the error are set so that the maximum LQPEs are $\beta_{E\max} = 10$ and $\beta_{E\max} = 15$, as it is given by (50).

One can see that the defocusing does not depend on the number of looks, as it has been predicted and explained in Section 6, but obviously depends on the error value $\beta_{E\max}$.

The effect of the non-uniform distribution of the shifts of single-look SAR images, described in Section 6, can be observed in Fig. 15. The single-look SAR images are shifted with a higher probability closer to the extreme values determined by the maximum LLPE (50a). The resulting multi-look SAR images show the appearance of two brighter points at the opposite ends of the defocused images of point targets. This effect is more evidently illustrated in Fig. 16, where the azimuth profiles are plotted for the point target indicated by the arrow in Figs. 13, 14(a), and 15(a). The two peaks on the profile for the harmonic error correspond to the peaks in the simulated multi-look SAP in Fig. 12.

8. CONCLUSION

The degradation of the resolution of the single-look and the multi-look SAPs caused by the uncompensated phase errors is considered in details and thoroughly illustrated by the numerical simulations. The new approach is proposed to characterize the influence of the

phase error in terms of its local linear and local quadratic phase errors (LLPE and LQPE). Based on this approach, the approximate analytical expressions have been derived to describe the azimuth resolution degradation. The efficiency of the method is demonstrated on two important practical examples: the quadratic and the harmonic phase errors presented on the multi-look processing interval.

REFERENCES

1. Oliver, C. and S. Quegan, *Understanding Synthetic Aperture Radar Images*, Artech House, Norwood, MA, 1999.
2. Carrara, W. G., R. S. Goodman, and R. M. Majewski, *Spotlight Synthetic Aperture Radar: Signal Processing Algorithms*, Artech House, Boston, London, 1995.
3. Cumming, I. G. and F. H. Wong, *Digital Processing of Synthetic Aperture Radar Data: Algorithms and Implementation*, Artech House, Norwood, MA, 2005.
4. Franceschetti, G. and R. Lanari, *Synthetic Aperture Radar Processing*, CRC Press, 1999.
5. Bezvesilniy, O. O. and D. M. Vavriv, "Synthetic aperture radar systems for small aircrafts: Data processing approaches," *Recent Advances in Aircraft Technology*, Chapter 20, 465–498, R. K. Agarwal Ed., InTech, Croatia, 2012.
6. Vavriv, D. M. and O. O. Bezvesilniy, "Developing SAR for small aircrafts in Ukraine," *Proceedings of the 2011 IEEE MTT-S International Microwave Symposium (IMS 2011)*, 1–4, Baltimore, USA, Jun. 5–10 2011.
7. Bezvesilniy, O. O., I. M. Gorovyi, S. V. Sosnytskiy, V. V. Vinogradov, and D. M. Vavriv, "Multi-look stripmap SAR processing algorithm with built-in correction of geometric distortions," *Proceedings of the European Conference on Synthetic Aperture Radar (EUSAR 2010)*, 712–715, Aachen, Germany, Jun. 7–10, 2010.
8. Bezvesilniy, O. O., I. M. Gorovyi, S. V. Sosnytskiy, V. V. Vinogradov, and D. M. Vavriv, "SAR processing algorithm with built-in geometric correction," *Radio Physics and Radio Astronomy*, Vol. 2, No. 3, 277–286, 2011.
9. Bezvesilniy, O. O., I. V. Dukhopelnykova, V. V. Vinogradov, and D. M. Vavriv, "Retrieving 3-D topography by using a single-antenna squint-mode airborne SAR," *IEEE Transactions on Geoscience and Remote Sensing*, Vol. 45, No. 11, 3574–3582, 2007.
10. Bezvesilniy, O. O., I. M. Gorovyi, V. V. Vinogradov, and

D. M. Vavriv, "Multi-look radiometric correction of SAR images," *Radio Physics and Radio Astronomy*, Vol. 3, No. 2, 169–177, 2012.

11. Bezvesilniy, O. O., I. M. Gorovyi, and D. M. Vavriv, "Estimation of phase errors in SAR data by local-quadratic map-drift autofocus," *Proceedings of the 13th International Radar Symposium (IRS-2012)*, 376–381, Warsaw, Poland, May 23–25, 2012.
12. Bezvesilniy, O. O., I. M. Gorovyi, and D. M. Vavriv, "Local-quadratic map-drift autofocus for synthetic aperture radars," *Radio Physics and Radio Astronomy*, Vol. 3, No. 4, 365–375, 2012.
13. Curlander, J. C., et al., "Fundamentals and special problems of synthetic aperture radar," AGARD Lecture Series, 1992.
14. Brown, W. M., "SAR resolution in the presence of phase errors," *IEEE Transactions on Aerospace and Electronic Systems*, Vol. 24, No. 6, 808–814, 1988.
15. Fornaro, G., G. Franceschetti, and S. Perna, "Motion compensation errors: Effect on the accuracy of airborne SAR images," *IEEE Transactions on Aerospace and Electronic Systems*, Vol. 41, No. 4, 1338–1352, 2005.
16. Fornaro, G., "Trajectory deviations in airborne SAR: Analysis and compensation," *IEEE Transactions on Aerospace and Electronic Systems*, Vol. 35, No. 3, 997–1009, 1999.
17. Marechal, N., "High frequency phase errors in SAR imagery and implications for autofocus," *International Geoscience and Remote Sensing Symposium (IGARSS 96)*, Vol. 2, 1233–1240, USA, 1996.
18. Sheng, W., T. Lv, and J. Cao, "The deviation in the phase of SAR echoes due to INS error," *Chinese Journal of Electronics*, Vol. 18, No. 1, 177–182, 2009.
19. Mao, Y., "Error analysis of SAR motion compensation," *IEEE International Conference on Imaging Systems and Techniques (IST)*, 377–380, Beijing, China, 2012.
20. Zelenka, J. S., "SAR image quality effects of damped phase and amplitude errors," *Proceedings of the IEEE National Radar Conference*, 61–67, USA, 1988.
21. Koo, V. C., Y. K. Chan, G. Vetharatnam, M. Y. Chua, C. H. Lim, C.-S. Lim, C. C. Thum, T. S. Lim, Z. bin Ahmad, K. A. Mahmood, M. H. Bin Shahid, C. Y. Ang, W. Q. Tan, P. N. Tan, K. S. Yee, W. G. Cheaw, H. S. Boey, A. L. Choo, and B. C. Sew, "A new unmanned aerial vehicle synthetic aperture radar for environmental monitoring," *Progress In Electromagnetics Research*, Vol. 122, 245–268, 2012.